Testing extreme ultraviolet optics with visible-light and extreme ultraviolet interferometry

Kenneth A. Goldberg[a] and Patrick Naulleau
Center for X-ray Optics, Lawrence Berkeley National Laboratory, Berkeley, California 94720

Jeffrey Bokor
Center for X-Ray Optics, Lawrence Berkeley National Laboratory and EECS Department, University of California, Berkeley, California 94720

Henry N. Chapman and Anton Barty
Lawrence Livermore National Laboratory, Livermore, California 94550

(Received 28 May 2002; accepted 30 September 2002)

Optics for extreme ultraviolet (EUV) lithography arguably have the most strict fabrication tolerances of any optical systems fabricated to date, and the development of EUV lithography pushes advanced optical fabrication techniques toward never before realized levels of figure accuracy and finish quality. As EUV lithography advances toward viability, the need for ultrahigh-accuracy wave front metrology tools has never been greater. To enable the development of diffraction-limited EUV optical systems, visible-light and EUV interferometries must work in close collaboration. We present a detailed comparison of EUV and visible-light wave front measurements performed across the field of view of a lithographic-quality projection optical system designed for use in the Engineering Test Stand developed by the Virtual National Laboratory and the EUV Limited Liability Company. The comparisons reveal that the present level of root mean square agreement lies in the 0.3–0.4 nm range, with an agreement of 0.15 ± 0.03 nm, excluding astigmatism. Astigmatism is the most significant aberration component for the alignment of this optical system; it is also the dominant term in the discrepancy, and the aberration with the highest measurement uncertainty. With EUV optical systems requiring total wave front quality in the $\lambda_{EUV}/50$ (0.25 nm) range, and even higher surface-figure quality for the individual mirror elements ($\sim$0.1 nm), improved accuracy through future comparisons, and additional studies, are required.
 [DOI: 10.1116/1.1523401]

I. INTRODUCTION

Diffraction-limited optical systems designed for extreme ultraviolet (EUV) lithography operate with 13 nm wavelength light and have total system wave front error tolerances in the $\lambda_{EUV}/50$ (0.25 nm) range, for the low-spatial-frequency, or figure aberrations. Multiple multilayer-coated reflective optical elements are combined to form a single compound projection lens for EUV lithography. To date, the designs of these systems have included two-element small-field-of-view optics for research purposes and larger, three, four, and six-element optical systems with wide, arc-shaped ring fields of view. For every reflective EUV optic, the combined system wave front at each point in the field depends on the surface profile and alignment of each mirror, and on the spatially varying multilayer-coating properties.

Within the Virtual National Laboratory,[1] two separate interferometers have been constructed to measure the system wave front and perform fine alignment of the projection optics designed for the Engineering Test Stand (ETS)[2] now operational at Sandia National Laboratories. Two four-mirror ring-field optical systems, referred to as the ETS Set-1 and Set-2 optics, have been fabricated for the ETS and inspected with both EUV and visible-light interferometry. The interferometers are a visible-light phase-shifting diffraction interferometer (PSDI)[3] at Lawrence Livermore National Laboratory (LLNL), and an EUV phase-shifting point diffraction interferometer (PS/PDI)[4] at Lawrence Berkeley National Laboratory (LBNL). These interferometers both operate on the principle of point diffraction to produce spherical reference wave fronts, and both are capable of measuring the system wave front at arbitrary positions across the ring field of view. The measurement of the Set-1 optic was performed in 1999–2000 and has been reported previously.[5,6] This paper describes the comparison of visible-light and EUV wave front measurements of the ETS Set-2 optic.

The primary goal of the comparison is to reach an objective evaluation of the level of agreement between these two interferometers, considering their respective measurements as separate and independent. In our tests, the average level of root mean square (rms) surface-figure agreement between the EUV PS/PDI and the visible-light PSDI is 0.35 ± 0.11 nm. For this off-axis reflective optical system, astigmatism is the dominant aberration term used in the alignment process. Astigmatism has also been the most challenging aberration to measure accurately: it comprises the majority of the wave front discrepancy in these comparisons.

[a]Electronic mail: kagoldberg@lbl.gov

II. TWO INTERFEROMETERS

The EUV PS/PDI and visible-light PDSI interferometers were constructed to evaluate the system wave front at positions across the field of view. While both interferometers can also measure distortion (image placement error), only the visible-light interferometer has been calibrated to do so. Measurements of the field-dependent optical performance provide feedback for the alignment of the individual mirrors. Detailed descriptions of the PS/PDI,[4,5] the PSDI,[3,7] and the alignment algorithm[3] have been published previously.

The EUV interferometer's light source is an undulator beamline at the Advance Light Source synchrotron radiation facility in Berkeley, California.[8] The source is tunable with a bandwidth $\lambda/\Delta\lambda$ of approximately 200. Based on the measured peak transmission wavelength of the ETS Set-2 optic, the interferometer was operated at 13.35 nm wavelength. The visible-light interferometer's light source is a Spectra Physics short coherence length frequency-doubled yttrium–aluminum–garnet laser operating at a wavelength of 532.2 nm with a longitudinal coherence length of approximately 5 mm.

The two interferometers operate at the same design temperature of 21 °C, within temperature-controlled environments to guarantee temperature stability better than 0.1 °C during the measurements.

The EUV measurements are performed in a vacuum environment constructed with ultrahigh vacuum materials and practices. The system operates at a base pressure of 10^{-7} Torr, with a partial pressure of oxygen gas of 3×10^{-5} Torr as a carbon-mitigation measure.

The alignment algorithm and measurement procedure specify 45 predefined field positions arranged into nine columns of five points. Both interferometers utilize their own lithographically fabricated pinhole arrays to define the field point measurement positions *in situ*. A substantial effort was made to guarantee that the field positions, and with them their conjugate positions, in the EUV and visible-light interferometers were closely matched. The ETS optics' housings are constructed with a *metrology tower* containing three capacitance micrometers for height and tilt sensing, and two, in-vacuum microscope cameras for lateral positions sensing.[9] Both the visible-light and EUV interferometry object-side pinhole arrays are fabricated onto monolithic substrates using lithography techniques that allow the individual pinholes to be placed to submicron accuracy with respect to fiducials on the masks; the fiducial positions are observed with the cameras on the metrology tower. The lateral positioning accuracy is approximately 10 μm, well within the 100 μm tolerance set by the alignment algorithm.

III. WAVE FRONT MEASUREMENTS

Wave front and distortion measurements were first performed with visible light as the system alignment was optimized. Between the visible light and EUV measurements, the ETS Set-2 optic was transported by truck from LLNL to LBNL in a specially designed shipping container, (the distance is approximately 45 miles). For both interferometers, data collection during the full-field measurement requires approximately 6 h.

The measured wave front quality data quoted herein are based solely on the low-spatial-frequency surface-figure aberrations, as determined by the first 37 Zernike polynomial terms: here, the ordering of the polynomials follows the FRINGE Zernike convention.[10] Tilt and defocus aberrations are currently only meaningful in the visible-light interferometer where the three-dimensional coordinates of the pinholes are accurately known. Although these aberrations are required for system alignment, they, along with piston, are excluded from the wave front analysis.

Visible-light wave front measurements at each field point include the average of six 32 iteration phase-shifting series, where each series uses 7–9 phase steps. The EUV wave front measurements use a single phase-shifting series with five steps at each field position. For each wave front measurement, a 37-term Zernike polynomial fit is performed on the raw wave front data to determine the surface figure (low spatial-frequency only). The interferogram analysis and wave front fitting procedures have been described previously.[5] The fit coefficients of the individual Zernike polynomials are reported using the rms convention: here a coefficient magnitude of 1 nm represents a 1 nm rms contribution from a given aberration term.

In both interferometers, the analysis is complicated by the motion and rotation of the projected pupil onto the stationary charge coupled device cameras. Owing to the non-normal angle of incidence of the beam onto the pupil's aperture (situated on the circular, on-axis, third mirror element), the wave front subtends a slightly elliptical domain with 0.9% eccentricity. The EUV and visible-light wave fronts are evaluated using an intermediate set of aberration polynomials that are orthogonal on the measurement domain.

Using a two-pinhole null-test technique,[4] the accuracy of the EUV PS/PDI technique has been demonstrated to be in the sub-$\lambda_{EUV}/200$, 0.06 nm range within a 0.1 numerical aperture. The accuracy of the visible-light PSDI is inferred from the comparison.

A. Comparison

Comparisons of visible-light and EUV measurements at the same field position are based on the difference wave front, defined as the subtractive difference of the two independent wave front measurements, reconstructed on the same domain using the Zernike fitting coefficients. Comparisons are made at 43 of the 45 predefined field point positions; two points are excluded from the visible-light data because of pinhole quality concerns. The field-point numbering convention assigns consecutive numbers to adjacent points in a column, from the outer edge inward. Field point zero occurs at approximately 15° counterclockwise from the center position, when looking upward into the optic from the wafer side, with the arc curving downward.

Figure 1 contains a side-by-side visible-light and EUV wave front comparison from two arbitrarily chosen field points. The EUV data, recorded with the PS/PDI, has a lower

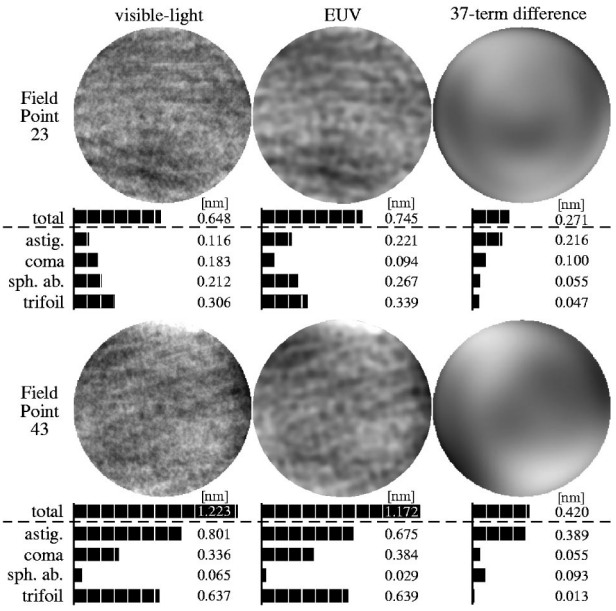

FIG. 1. Side-by-side visible-light and EUV wave front comparison from two arbitrarily chosen field points, shown on a grayscale range [−5.0, 5.0] nm. rms magnitudes of four aberration terms and the overall wave front error are given below each wave front. The third column contains the (subtractive) difference wave fronts reconstructed from a 37 term Zernike polynomial fit, shown on a grayscale range [−1.5, 1.5] nm.

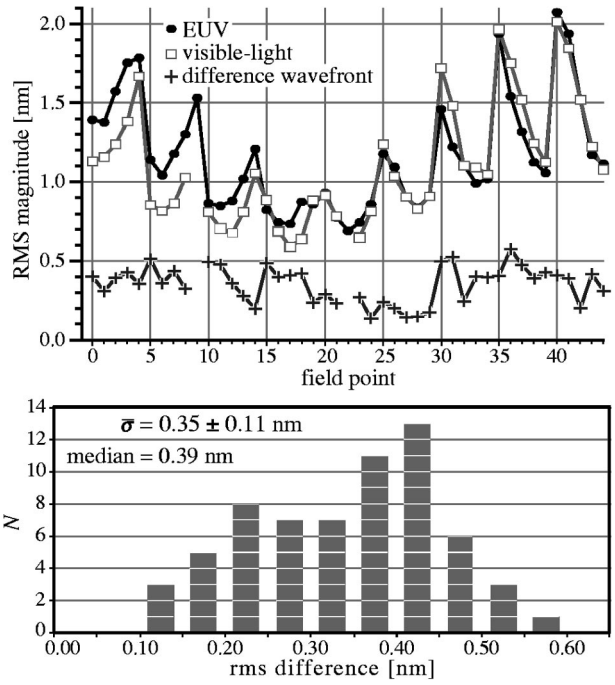

FIG. 2. EUV, visible-light, and difference-wave front rms magnitudes across the field of view. A histogram of the difference wave front rms magnitudes (lower) shows the overall level of agreement in the wave front comparison.

spatial-frequency bandwidth than the visible-light data because the EUV light passes through a 3-μm-wide image plane window. The window behaves as a low-pass spatial filter but does not affect the measurement of the much lower-frequency aberration terms of interest here. The wave front data are represented on a grayscale covering the range [−5.0, 5.0] nm. The rms magnitudes of four aberration terms and the overall wave front error are given below each wave front. The amplitudes of the first 37 Zernike polynomial terms (excluding tilt and defocus) are added as the root sum of squares to form the overall rms magnitude. The corresponding difference wave fronts are shown in the third column of Fig. 1, scaled on the range [−1.5, 1.5] nm and reconstructed from the first 37 Zernike polynomials. Each wave front shows some residual low-spatial-frequency aberrations, such as astigmatism, coma, etc.

A comparison of the rms aberration magnitudes of the individual measured wave fronts, and for the difference wave fronts, is shown in Fig. 2 for all of the measured field points. The aberration coefficients vary smoothly across the field of view: the sawtooth appearance in the plots comes from unwrapping the nine columns of points into a single vector of coefficients.

Analysis of the difference wave front rms magnitudes shows that the level of agreement between the two interferometers, averaged across the field, is 0.35 ± 0.11 nm (0.35 nm is approximately $\lambda_{EUV}/38$), with a median value of 0.39 nm, and spans a range of 0.14–0.58 nm. A histogram of the wave front difference rms magnitudes is also shown in Fig. 2.

The plots and contours in Fig. 3 isolate three of the individual aberration components: here, astigmatism, and a higher-ordered spherical aberration term are shown. Additional aberration coefficient data have been published elsewhere.[11] For these comparisons, the quantities of interest are the field-averaged mean difference $\bar{\Delta}$ and its standard deviation σ_Δ.

The majority of the discrepancy is concentrated in the low-spatial-frequency aberration terms, particularly astigmatism. For most of the Zernike terms, the field-averaged level of agreement is below $\lambda_{EUV}/1000$, with larger standard deviation magnitudes in the range of 0.3 down to 0.15 nm ($\lambda_{EUV}/50$ to $\lambda_{EUV}/90$). Yet for astigmatism, the relatively large $\bar{\Delta}$ values (0.280 ± 0.149 nm for Z_4, and 0.053 ± 0.091 nm for Z_5) indicate the presence of an important systematic difference between the two interferometers.

At this time, several potential sources of the discrepancy are being considered, with efforts concentrated in characterizing various error sensitivities in the visible-light interferometer. Analysis performed with the ETS Set-2 optic reinstalled in the PSDI uncovered critical sensitivities in the pinhole illumination conditions. In particular, the polarization direction and the wave front quality of the illuminating beam were found to contribute astigmatism errors up to 0.5 nm rms. Variations in the magnitudes of these effects from one field point to another raise concerns about the pinhole size and shape as additional error sources.

By restricting the NA (and the aberrations) of the pinhole-illuminating optics, and by performing a polarization averaging the contributions of these error sources can be significantly reduced. Because the optical system was mechanically realigned prior to these visible-light tests, there is no oppor-

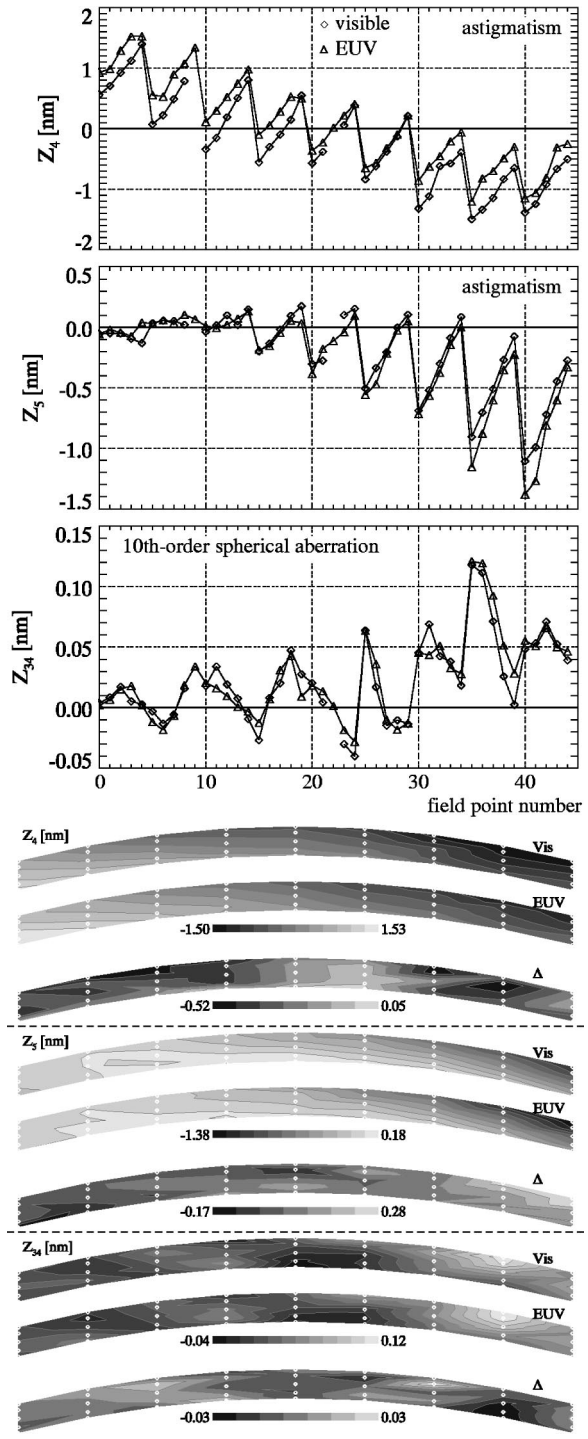

FIG. 3. Comparison of three EUV and visible-light wave front aberration coefficients across the field of view. The astigmatism terms are those for which the discrepancy is largest. The excellent agreement in the sensitive higher-ordered spherical term (and many other terms not shown) indicate that the field-point positions between the two interferometers are well aligned. The contours contain the same data as the plots, and include the difference values (Δ) as well.

tunity for subsequent meaningful comparisons of the visible-light and EUV wave front measurements.

B. Field position uncertainty

One challenge for the intercomparison of wave front measurements recorded on different interferometers is to guarantee that the field points where the measurements are performed are well matched between the different interferometers. Since the wave front is spatially varying across the field, a discrepancy in the field positions would introduce some level of difference.

Great care was taken to ensure that the field points used in the visible-light and EUV interferometers are well matched, to the level required by the alignment algorithm and by this intercomparison (tens of microns). If there were a significant field-point-position discrepancy, the observed wave front difference would contain a shear term related to the gradient of the changing wave front, including contributions from each mirror surface and a parallax from the displaced measurement points. That shear would most severely impact the aberration terms with the highest spatial frequency, i.e., those with the highest local slope. The high level of agreement in the higher-ordered aberration terms, compared to the lower-ordered terms, leads to the conclusion that field-position discrepancies are not contributing to the measurement discrepancy observed in the lower-ordered aberration terms.

C. EUV measurement precision and accuracy

The uncertainty in the EUV wave front measurements is calculated by studying the individual, single-exposure wave front measurements from within phase-shifting series. Fringe analysis and wave front fitting are performed on the individual measurements, and the standard deviation of the coefficients is calculated at each field point. The field average of those standard deviations is what we call the uncertainty in each coefficient. Except for astigmatism, the coefficient uncertainty is consistently below the $\lambda_{EUV}/1000$ level. Uncertainty in the two astigmatism terms is 0.024 and 0.014 nm, respectively ($\lambda_{EUV}/566$ and $\lambda_{EUV}/963$).

The accuracy of the EUV PS/PDI has been studied using an *in situ* null test technique.[4] Within a numerical aperture of 0.088, previous measurements have revealed spherical reference wave front accuracy levels of 0.04 nm rms ($\lambda_{EUV}/330$). Because the interferometer uses spatial filtering to produce the reference waves, the accuracy of the PS/PDI generally improves with the quality of the test wave front being evaluated. Thorough analysis of null-test measurements recorded during the EUV interferometry has not been completed; preliminary analysis suggests an uncalibrated rms systematic aberration magnitude of approximately $\lambda_{EUV}/200$ of 0.065 nm within 0.1 NA. The higher accuracy in prior measurements likely reflects a combination of the smaller NA and a different wave front error in the optical system under test.

Ultimately, it is through printing that the accuracy and predictive power of the interferometric measurements are verified. The EUV PS/PDI interferometry system was modified to enable static, small-field imaging experiments with controllable illumination coherence.[12] Imaging experiments conducted on the ETS Set-2 optic, after the EUV interferometry, have qualitatively verified the low predicted astigmatism near the center of the field of view.[13,14]

D. Measurement of low- and high-spatial-frequency aberrations

One unexpected outcome of the interferometry comparison is the fact that the highest spatial frequency aberration terms are those for which the comparison is best. Furthermore, the uncertainty in the EUV wave front measurements is greater for the low-spatial-frequency aberrations than for the higher-spatial-frequency aberrations. It is possible that the variation of low-spatial-frequency aberrations is an inherent challenge associated with point-diffraction class interferometers (visible and EUV) in which the quality of the diffracted wave front depends on diffraction from a tiny aperture. While interferometers that use point diffraction may effectively filter the higher-spatial frequency aberrations from the reference wave front, they may be vulnerable to vibration, small displacements between measurements, pinhole-shape irregularities, and inadequate spatial filtering. Since it is usually these low-spatial-frequency aberrations that require the highest accuracy in a system alignment process, this issue deserves further study.

IV. CONCLUSION

To date, EUV interferometry performed with the phase-shifting point diffraction interferometer is the most accurate predictor of lithographic performance available for the measurement of EUV optical systems. Through ongoing intercomparisons of developmental visible-light and EUV wave front metrology techniques with an accuracy standard such as the PS/PDI, the commodity of high accuracy can be distributed to the many groups working to create EUV optical systems.

The direct comparison of EUV and visible-light interferometric measurements of the ETS Set-2 optical system represents one part of the effort to identify systematic differences among interferometers and improve the accuracy of all interferometry for EUV applications. Our measurements show that the level of agreement achieved thus far is 0.35 ± 0.11 nm rms. Astigmatism comprises the majority of the difference. When the astigmatism contribution is excluded, the field-averaged difference-wave front rms magnitude reduces to 0.15 ± 0.03 nm.

Recently, several critical yet likely remediable wave front measurement error sources have been identified in the PSDI. Error sensitivities as large as 0.5 nm rms are attributable to variations in the pinhole illumination conditions in the interferometer, and may thus be largely responsible for the EUV/visible-light discrepancies described in this article. While efforts to eliminate or reduce these error sources appear to be successful, subsequent comparisons with EUV interferometry will not be possible because the optical system has also undergone a significant mechanical realignment to reduce the large aberrations magnitudes at the edges of the field.

The importance of continued improvement and ongoing research in high-accuracy interferometry is clear from the fact that the required accuracy is beyond the level that is available and has been demonstrated today. Interferometers suitable for testing $\lambda_{EUV}/50$ quality EUV optical systems (0.25 nm wave front error) must have an accuracy at least several times better: the level of EUV-visible interferometry agreement will have to be improved to below 0.1 nm (improved perhaps by a factor of 5 or more) in the next several years.

In practice, the agreement between visible-light and EUV measurements of the same EUV optical system relies on nearly ideal quality and well-characterized multilayer coatings.[15] As we have demonstrated previously, the presence of carbon contamination on a mirror's surface can create a significant difference between the measured visible-light and EUV reflected phase (and amplitude).[16] This issue may have to be addressed if and when EUV optical systems are realigned after some period of use. The polarization of illuminating beams can also affect wave front measurements made by both EUV and visible-light interferometers; these design-dependent effects typically grow more important with larger internal angles. When the multilayer coatings are well characterized, the polarization dependence will be predictable.

In addition to the wave front measurements that are presented here, complete characterization of a lithographic optical system requires the measurement of both wave front quality and distortion. At this time, only the visible-light interferometer has been configured for distortion measurements, the accuracy of which is verifiable only through printing well-calibrated large-field masks, a subject of ongoing research in the ETS.

ACKNOWLEDGMENTS

The authors are grateful for the hard work and contributions of the Center for X-Ray Optics engineers and staff including Paul Denham, Keith Jackson, Senajith Rekawa, Kevin Bradley, Brian Hoef, Farhad Salmassi, David Richardson, M. Gideon Jones, Nord Anderson, Drew Kemp, René Delano, Lon Amerman, and David Attwood. They are also indebted to Erik Anderson for electron beam lithography support and development of the pinhole arrays, and to Dino Ciarlo of LLNL for wafer processing. Additional thanks are due for the contributions of LLNL staff in the operation and upgrade of the visible-light interferometer, including Daren Dillon, Nhan Nguyen, Rick Montesanti, Todd Decker, Terry Swan, Carl Chung, Layton Hale, and Gary Otani. This research has been supported by the Extreme Ultraviolet Limited Liability Company (EUV LLC),[17] the DARPA Advanced Lithography Program, and by the Office of Basic Energy Sciences of the U.S. Department of Energy.

[1]The Virtual National Laboratory is the name given to the collaboration between Lawrence Berkeley, Lawrence Livermore, and Sandia National Laboratories.
[2]D. A. Tichenor *et al.*, Proc. SPIE **3997**, 48 (2000).
[3]H. N. Chapman and D. W. Sweeney, Proc. SPIE **3331**, 102 (1998).
[4]P. P. Naulleau, K. A. Goldberg, S. H. Lee, C. Chang, D. Attwood, and J. Bokor, Appl. Opt. **38**, 7252 (1999).
[5]K. A. Goldberg, P. Naulleau, P. J. Batson, P. Denham, J. Bokor, and H. N. Chapman, Proc. SPIE **3997**, 867 (2000).
[6]K. A. Goldberg, P. Naulleau, P. Batson, P. Denham, H. Chapman, and J. Bokor, J. Vac. Sci. Technol. B **18**, 2911 (2000).
[7]G. E. Sommargren, U.S. Patent No. 5,548,403 (August 20, 1996).

[8]D. T. Attwood *et al.* IEEE J. Quantum Electron. **35**, 709 (1999).
[9]P. P. Naulleau, P. J. Batson, P. E. Denham, and M. S. Jones, U.S. Patent No. 6,327,102 (March, 2000).
[10]J. S. Loomis, *FRINGE User's Manual* (Optical Sciences Center, University of Arizona Press, Tuscon, AZ, 1976).
[11]K. A. Goldberg, P. Naulleau, J. Bokor, and H. N. Chapman, Proc. SPIE **4688**, 329 (2002).
[12]P. Naulleau, K. Goldberg, E. Anderson, P. Batson, P. Denham, S. Rekawa, and J. Bokor, Proc. SPIE **4343**, 639 (2001).
[13]P. Naulleau *et al.*, Proc. SPIE **4688**, 64 (2002).
[14]P. Naulleau *et al.*, J. Vac. Sci. Technol. B these proceedings.
[15]R. Soufli *et al.*, Proc. SPIE **4343**, 51 (2001).
[16]K. A. Goldberg, P. Naulleau, S. H. Lee, C. Chang, C. Bresloff, R. Gaughan, H. N. Chapman, J. Goldsmith, and J. Bokor, Proc. SPIE **3676**, 635 (1999).
[17]The EUV Limited Liability Company (EUV LLC) comprises member companies: Intel, AMD, Motorola, IBM, Infineon, and Micron Technology.